Valence and spin states, and the metal-insulator transition in ferromagnetic La$_{2-x}$Sr$_x$MnNiO$_6$ ($x=0,0.2$)

J.-S. Kang,[1,*] H. J. Lee,[1] D. H. Kim,[1] S. Kolesnik,[2] B. Dabrowski,[2] K. Świerczek,[3] Jieun Lee,[4]
Bongjae Kim,[4] and B. I. Min[4,†]

[1]*Department of Physics, The Catholic University of Korea, Bucheon 420-743, Korea*
[2]*Department of Physics, Northern Illinois University, DeKalb, Illinois 60115, USA*
[3]*AGH University of Science and Technology, 30-059 Krakow, Poland*
[4]*Department of Physics, Pohang University of Science and Technology, Pohang 790-784, Korea*

Electronic structures of a ferromagnetic insulator La$_2$MnNiO$_6$ and Sr-doped La$_{1.8}$Sr$_{0.2}$MnNiO$_6$ have been investigated by employing soft x-ray synchrotron-radiation spectroscopies, first-principles band-structure calculations, and ligand-field multiplet calculations. Our study provides evidence that La$_2$MnNiO$_6$ has the [high-spin (HS) Mn^{4+}-$^3A_2$ Ni^{2+}] configuration while La$_{1.8}$Sr$_{0.2}$MnNiO$_6$ has [HS Mn^{4+}-$^3A_2$ Ni^{2+} low-spin Ni^{3+}]. It is directly observed that the spin moments of Mn and Ni ions are coupled ferromagnetically. The metallic spectral weight is observed for $x=0.2$ in O $1s$ x-ray absorption spectroscopy, which is consistent with the half-metallic ground state predicted by band-structure calculations.

Double perovskite La$_2$MnNiO$_6$ is interesting due to its highest Curie temperature $T_C \sim 280$ K among ferromagnetic (FM) insulators.[1,2] It also exhibits both the magnetoresistance and magnetocapacitance effects,[3] which offer the potential for spintronic devices. Despite extensive studies on magnetic properties of La$_2$MnNiO$_6$, however, the valence and spin states of Mn and Ni ions in La$_2$MnNiO$_6$ are still controversial, whether they are in the [Mn^{3+}-Ni^{3+}] configuration[4–7] or in the [Mn^{4+}-Ni^{2+}] configuration.[1,2,8–13] There are also reports that the valence states of Mn and Ni ions in La$_2$MnNiO$_6$ vary between the above two configurations, depending on the synthesis conditions of samples, such as annealing and oxygen partial pressure.[14,15] In fact, depending on the temperature, there are various stable structures for La$_2$MnNiO$_6$, such as orthorhombic (*Pbnm*), rhombohedral ($R\bar{3}, R\bar{3}m$), and monoclinic ($P2_1/n$). The coexistence of orthorhombic and rhombohedral phases was observed with $T_C \approx 150$ K and $T_C \approx 280$ K, respectively.[9,14] Then it was speculated[14] that the low-T_C orthorhombic phase contained [Mn^{4+}-Ni^{2+}] while the high-T_C rhombohedral phase contained [Mn^{3+}-Ni^{3+}]. On the other hand, it is worthwhile to explore the effect of doping carriers in a ferromagnetic insulator La$_2$MnNiO$_6$ to see whether the doped La$_2$MnNiO$_6$ becomes a metallic ferromagnet similarly as in colossal magnetoresistance manganite La$_{1-x}$Sr$_x$MnO$_3$. For this purpose, we have studied physical properties of Sr-doped La$_{2-x}$Sr$_x$MnNiO$_6$, which corresponds to the hole-carrier doping.

In this work, we have addressed the issue of the valence states and the spin configurations of Mn and Ni ions in La$_{2-x}$Sr$_x$MnNiO$_6$ ($x=0,0.2$) and have investigated the possible metal-insulator transition with hole doping. By using soft x-ray absorption spectroscopy (XAS),[16–18] soft x-ray magnetic circular dichroism (XMCD),[19,20] and photoemission spectroscopy (PES),[21,22] we have studied the electronic structures of La$_{2-x}$Sr$_x$MnNiO$_6$ and determined the partial density of states (PDOS) and the spin configurations. We have also performed both ligand-field multiplet (LFM) cal-

culations and *ab initio* band-structure calculations to analyze experimental data.

Polycrystalline La$_{2-x}$Sr$_x$MnNiO$_6$ samples were prepared by a standard solid-state reaction method. Room-temperature neutron-diffraction experiments performed at Argonne's IPNS showed that La$_2$MnNiO$_6$ sample is a double perovskite with the ordered Mn/Ni sublattice. Two crystal structures are coexisting, 60% rhombohedral ($R\bar{3}$) and 40% monoclinic ($P2_1/n$). La$_{1.8}$Sr$_{0.2}$MnNiO$_6$ showed no evidence of the ordering of Mn/Ni cations and can be described with rhombohedral $R\bar{3}c$ space group. XAS, XMCD, and PES experiments were performed at two different chambers in the 2A undulator beamline of the Pohang Light Source (PLS).[23] Samples were cleaned *in situ* by repeated scraping with a diamond file. XAS and XMCD spectra were obtained at $T \sim 80$ K in the total electron yield mode and XMCD spectra were obtained under the magnetic field of ~ 0.4 T. The chamber pressure for PES was about 5×10^{-11} Torr and PES data were obtained at $T \sim 100$ K using a SCIENTA SES100 analyzer.

Figure 1(a) shows the temperature dependence of dc magnetization for La$_{2-x}$Sr$_x$MnNiO$_6$ measured in a high magnetic field of 5 T. The isothermal magnetization for $x=0$ in the inset of Fig. 1(a) shows a narrow hysteresis curve with the coercivity field of ~ 220 Oe at $T=5$ K and full saturation close to 5 μ_B/f.u. This latter value reflects the well-ordered Mn and Ni ions at B and B' sites of double perovskite A_2BB'O$_6$. Much lower magnetization (1.2 μ_B/f.u. at 5 K) is observed for $x=0.2$ without a clear tendency to saturation. The ac susceptibility, measured in the ac excitation field of 14 Oe at a frequency of 1 kHz, is presented in Fig. 1(b) for both samples. The $x=0$ sample demonstrates two close ferromagnetic transition temperatures (determined from the extreme slope of the curve) at 284 and 276 K. This suggests that both rhombohedral and monoclinic phases of our La$_2$MnNiO$_6$ have the very close T_C's. The $x=0.2$ sample shows a lower susceptibility with three well-separated transitions at 271, 250, and 164 K. In contrast, high magnetic
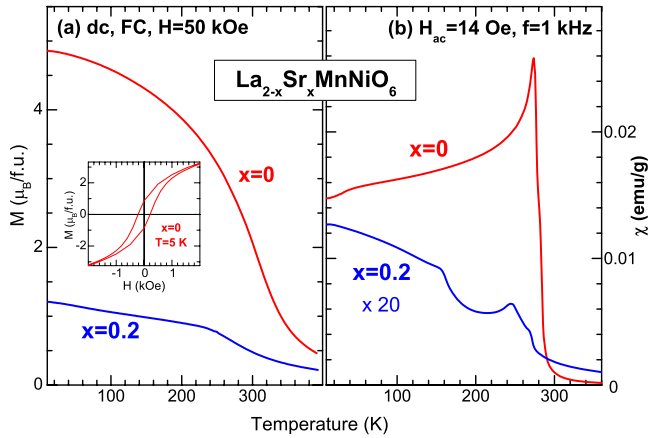
FIG. 1. (Color online) Temperature dependence of (a) dc magnetization and (b) the real part of ac susceptibility χ' for $La_{2-x}Sr_xMnNiO_6$. Inset: Isothermal magnetization at $T=5$ K for La_2MnNiO_6.

field magnetization in Fig. 1(a) shows only one transition at 312 and 269 K for $x=0$ and $x=0.2$, respectively.

Figure 2 shows the measured Mn and Ni $2p$ XAS spectra of $La_{2-x}Sr_xMnNiO_6$ ($x=0,0.2$). In Fig. 2(a), Mn $2p$ XAS spectra are compared to those of reference Mn oxides[24] of MnO_2 (Mn^{4+}),[25] Mn_2O_3 (Mn^{3+}),[26] MnO (Mn^{2+}),[25] and the calculated Mn $2p$ XAS, obtained by employing the LFM calculation. This calculation is for a Mn^{4+} ($3d^3$) ion under the octahedral (O_h) symmetry with $10Dq=2.4$ eV ($10Dq$: the crystal-field splitting energy between t_{2g} and e_g states), where two configurations of d^n and $d^{n+1}\underline{L}^1$ are considered ($n=3$ and $\underline{L}$: a ligand hole).[27] The present Mn $2p$ XAS spectrum for $x=0$ is similar to that of $LaMn_{0.5}Ni_{0.5}O_{3.05}$ in literature[11] and also to that of La_2MnNiO_6 thin film.[28] Note that the measured Mn $2p$ XAS spectra for $x=0$ and $x=0.2$ in Fig. 2(a) are close to each other, and are quite different from those of Mn_2O_3 and MnO, but qualitatively similar to that of MnO_2. Moreover, they are described well by the calculated
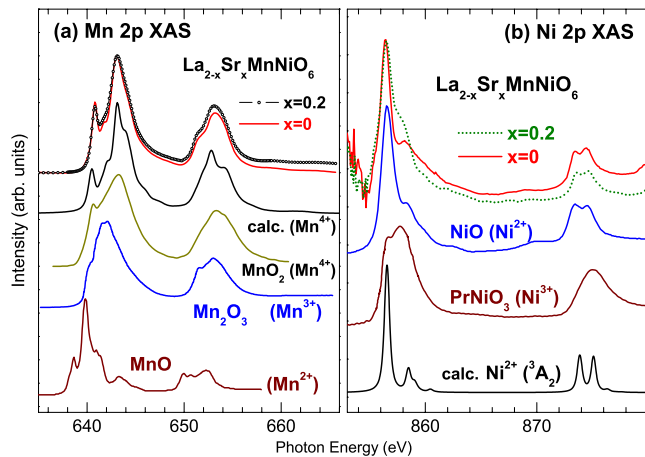

FIG. 2. (Color online) (a) Mn $2p$ XAS spectra of $La_{2-x}Sr_xMnNiO_6$, compared to the calculated Mn^{4+} XAS and those of reference Mn oxides. (b) The extracted Ni $2p$ XAS spectra of $La_{2-x}Sr_xMnNiO_6$, compared to those of reference Ni oxides and the calculated Ni^{2+} XAS.
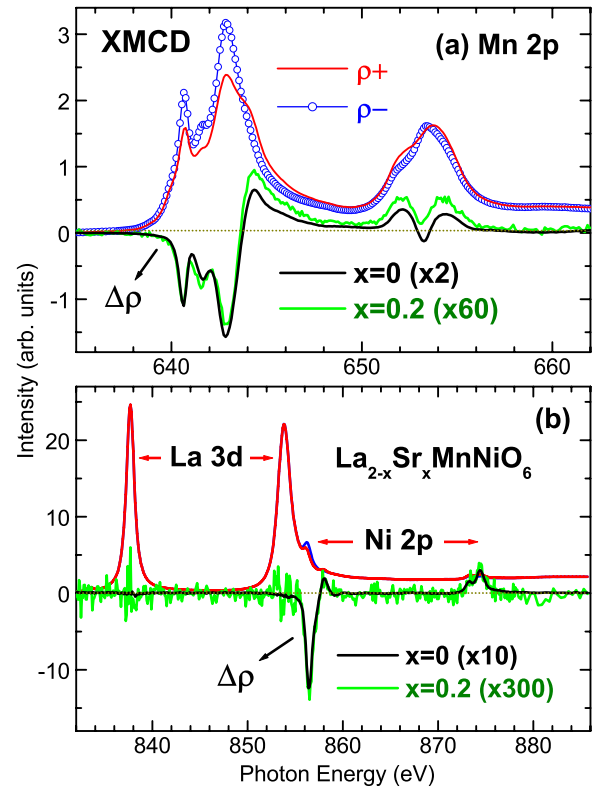

FIG. 3. (Color online) (a) Mn $2p$ absorption spectra obtained with different photon helicities, ρ_+ and ρ_-, and the XMCD spectrum, $\Delta\rho=\rho_+-\rho_-$, for La_2MnNiO_6. For $La_{1.8}Sr_{0.2}MnNiO_6$, only $\Delta\rho$ (green curve) is shown. (b) Similarly for the La $3d$ and Ni $2p$ states.

Mn^{4+} XAS, indicating that Mn ions are formally tetravalent.

The extracted Ni $2p$ XAS spectra of $La_{2-x}Sr_xMnNiO_6$ are shown in Fig. 2(b).[29] The Ni $2p$ XAS spectra of reference Ni oxides[30] are shown together, NiO (Ni^{2+}) (Ref. 31) and $PrNiO_3$ [low-spin (LS) Ni^{3+}].[32] The measured Ni $2p$ XAS spectrum for $x=0$ is very similar to that of NiO (Ni^{2+}) but quite different from that of $PrNiO_3$ (Ni^{3+}). Also shown at the bottom of Fig. 2(b) is the calculated Ni $2p$ XAS spectrum obtained from the LFM calculation. It is shown that the qualitative features of the Ni $2p$ XAS spectrum of NiO are described well by the calculated Ni $2p$ XAS for a Ni^{2+} ion ($^3A_2, S=1: t_{2g}^3\uparrow t_{2g}^3\downarrow e_g^2\uparrow$), with $10Dq=2.4$ eV. This provides evidence that Ni ions in La_2MnNiO_6 are nearly divalent. Further, the spin configuration of the occupied Ni $3d$ states corresponds to the LS configuration in the band picture, that is, the exchange splitting Δ_x between the $t_{2g}\uparrow$ and $t_{2g}\downarrow$ bands is smaller than the crystal-field splitting $10Dq$. Indeed this finding is consistent with the recent band-structure calculations.[33–35] Also our finding rules out the speculation[14] that La_2MnNiO_6 with the high-T_C rhombohedral phase might have the $[Mn^{3+}-Ni^{3+}]$ configuration.

The Ni $2p$ XAS spectrum for $x=0.2$ exhibits a higher intensity at the high-energy shoulder ($h\nu\approx858$ eV) than for $x=0$, the position of which coincides with the main peak in trivalent $PrNiO_3$ (Ni^{3+}). This suggests that there is some contribution from LS Ni^{3+} states in $x=0.2$. Note that Mn $2p$ XAS spectra in Fig. 2(a) hardly change with Sr doping, indicating that the decreased average valence state of the A
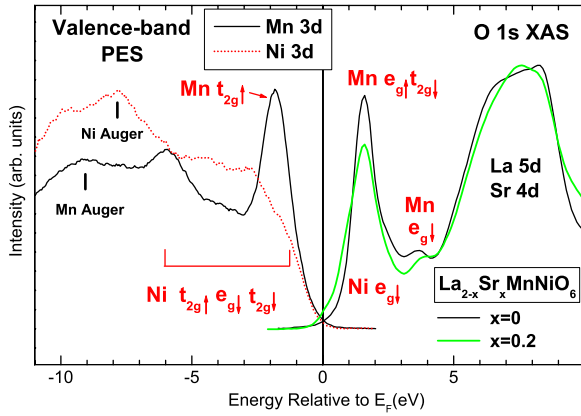
FIG. 4. (Color online) (Left) The Mn $3d$ PES and Ni $3d$ PES for La$_2$MnNiO$_6$. (Right) The O $1s$ XAS spectra of La$_{2-x}$Sr$_x$MnNiO$_6$.

FIG. 5. (Color online) (a) Comparison of the calculated Mn $2p$ XAS, obtained in the GGA+U and the GGA, with the measured XAS for La$_2$MnNiO$_6$. (b) Calculated Mn $3d$ and Ni $3d$ PDOS's for La$_{1.75}$Sr$_{0.25}$MnNiO$_6$, obtained in the GGA+U ($U=5.4$ eV).

site, induced by Sr-doping, is compensated by the increase in the Ni valence state. That is, for $x=0.2$, the hole carriers induced by Sr doping are created mainly at Ni sites.

Figure 3(a) shows the Mn $2p$ absorption spectra of La$_2$MnNiO$_6$ obtained with the photon helicity parallel (ρ_+) and antiparallel (ρ_-) to the applied magnetic field, respectively. The black curve shows the XMCD spectrum ($\Delta\rho=\rho_+-\rho_-$). Similarly, Fig. 3(b) shows ρ_+, ρ_-, and $\Delta\rho$ for the overlapped La $3d$ and Ni $2p$ states. Figure 3 reveals the following features. (i) The polarities of Mn $2p$ XMCD and Ni $2p$ XMCD are the same, indicating the parallel alignment of the spin moments between Mn and Ni ions. This finding is consistent with the ferromagnetic behavior of La$_{2-x}$Sr$_x$MnNiO$_6$. The very weak, but certainly clear, dichroism has been observed in O $1s$ XMCD (not shown in this paper), with the same polarity as those of Mn and Ni ions. (ii) The line shapes of the XMCD spectra for $x=0.2$ (green color) are very similar to those for $x=0$ but the XMCD signals are substantially lower ($\sim 1/30$) than in $x=0$. This trend is consistent with the disordered Mn/Ni ions in La$_{1.8}$Sr$_{0.2}$MnNiO$_6$. Note that, according to the simple super-exchange rules,[35] the magnetic interactions between Mn^{4+}-Mn^{4+} and Ni^{2+}-Ni^{2+} in cation-disordered La$_{1.8}$Sr$_{0.2}$MnNiO$_6$ are antiferromagnetic (AF) while those between Mn^{4+}-Ni^{2+} in cation-ordered La$_{1.8}$Sr$_{0.2}$MnNiO$_6$ is FM. Therefore the much weaker XMCD signals for $x=0.2$, as compared to $x=0$, reflect that the portion of the cation-disordered region is larger than that of the cation-ordered region. Much larger *bulk* magnetization, observed in Fig. 1, seems to be due to the use of much stronger magnetic field (5 T) than in XMCD (0.4 T). (iii) La $3d$ states show nearly no dichroism, in agreement with the expectation for trivalent La^{3+} ions having no $4f$ electrons.[29]

Figure 4 shows the valence-band PES spectra for the Mn $3d$ and Ni $3d$ states for La$_2$MnNiO$_6$ (left) and the O $1s$ XAS spectra of La$_{2-x}$Sr$_x$MnNiO$_6$ (right). The Mn $3d$ and Ni $3d$ PES spectra were determined from the Mn $2p\rightarrow3d$ resonant PES (RPES) and Ni $2p\rightarrow3d$ RPES, respectively.[29] The Mn $3d$ and Ni $3d$ PES spectra for $x=0.2$ are not shown in this figure but they are very similar to those for $x=0$.[36] The O $1s$ XAS spectrum represents the unoccupied Mn and Ni $3d$ states via the hybridization with the O $2p$ states. In
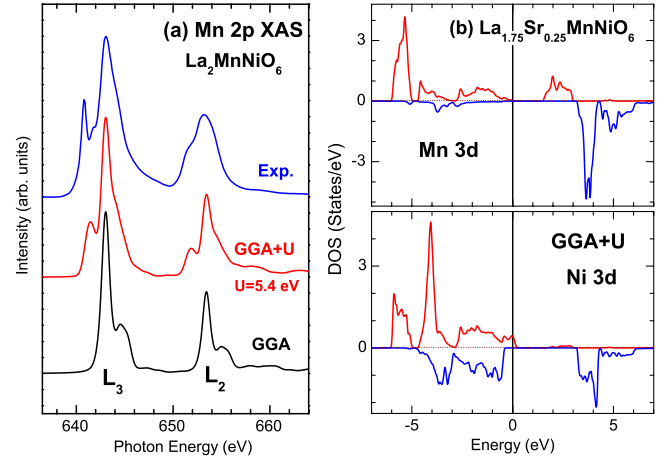
this figure, the O $1s$ XAS spectrum has been shifted by -529 eV to account for the O $1s$ binding energy. In PES, the sharp peak around -2 eV represents the occupied Mn $3d^3(t_{2g}^3\uparrow)$ states. Then the broad feature that extends from E_F to ~-5 eV represents the occupied Ni $3d^8(t_{2g}^3\uparrow t_{2g}^3\downarrow e_g^2\uparrow)$ states. The broad features between -5 and -10 eV are Mn and Ni Auger emissions.[29]

In O $1s$ XAS, the lowest-energy peak is identified as mainly the empty Ni $e_g\downarrow$ states overlapping the empty Mn $e_g\uparrow t_{2g}\downarrow$ states. Then the weak feature at a higher energy will correspond to the empty Mn $e_g\downarrow$ states. According to these assignments, the splitting between the lowest-energy peak and the next peak corresponds to the rough measure of the exchange splitting $\Delta_x\sim 2$ eV between Mn $e_g\uparrow$ and $e_g\downarrow$ states. Note that the spectral weight near E_F in O $1s$ XAS is larger for $x=0.2$ than $x=0$, suggesting that hole carriers are created in the Ni $e_g\uparrow$-O $2p$-hybridized orbitals for $x>0$. This will result in the metallic ground state for $x>0$, as compared to the ferromagnetic insulating ground state for $x=0$.[37]

Figure 4 confirms that Mn ions are in the Mn^{4+} states with the high-spin (HS) configuration ($t_{2g}^3\uparrow$) and that Ni ions are in the Ni^{2+} states with the $t_{2g}^3\uparrow t_{2g}^3\downarrow e_g^2\uparrow$ configuration. Then the topmost occupied states and the lowest unoccupied states have mainly the Ni $e_g\uparrow$ and Ni $e_g\downarrow$ character, respectively. Hence for $x>0$, hole carriers are expected to be created in the Ni $e_g\uparrow$-O $2p$-hybridized orbitals.

Figure 5(a) compares the calculated Mn $2p$ XAS for La$_2$MnNiO$_6$, based on the band-structure results, with the measured Mn $2p$ XAS. Band-structure calculations were performed in the generalized gradient approximation (GGA) and the GGA+U (U: effective Coulomb correlation between Mn and Ni $3d$ electrons). Both the GGA and the GGA+U ($U=5.4$ eV) produced the correct insulating band structures for La$_2$MnNiO$_6$. The spin-orbit splittings in the calculated Mn $2p$ XAS both in the GGA and the GGA+U are more or less consistent with that in experiment. However, the detailed shape from the GGA exhibits large discrepancies from experiment: the peak widths are much narrower than in experi-

ment and the shoulders are located at the higher-energy side of the main peaks. Such discrepancies are improved a lot in the GGA+U calculation, resulting in better agreement with experiment. This is due to the change in the unoccupied DOS of Mn^{4+}. In the GGA, the $e_g\uparrow$ and $t_{2g}\downarrow$ states almost overlap[35] while, in the GGA+U, the $t_{2g}\downarrow$ state is shifted higher in energy than the $e_g\uparrow$ state, as shown in the upper panel of Fig. 5(b). This finding indicates that one should take into account the Coulomb correlation effect properly when studying the electronic structures of $La_{2-x}Sr_xMnNiO_6$.

On the other hand, band-structure calculations for cation-ordered $La_{1.75}Sr_{0.25}MnNiO_6$ show that it becomes metallic with hole carriers mainly at Ni sites [see Fig. 5(b)]. The DOS at E_F comes mostly from Ni 3d states, whereas the contribution from Mn 3d states is negligible. In the Ni 3d PES spectrum for $x=0.2$, no clear metallic Fermi edge has been observed, which is contradictory to the calculated PDOS [Fig. 5(b)]. Such a discrepancy might be due to the contribution from the possible insulating surface layers in our Sr-doped sample. Interestingly, $La_{1.75}Sr_{0.25}MnNiO_6$ becomes half-metallic with 100% spin-polarization at E_F. This feature deserves to be verified by experiment. We have checked the effect of the cation antisite disorder on the electronic structure of $La_{1.75}Sr_{0.25}MnNiO_6$ by exchanging the positions of Mn and Ni ions in the ordered system. We have found that the total energy difference between the FM and AF states becomes negligible and that the half-metallic nature is robust to the antisite disorder.

In conclusion, Mn ions are formally tetravalent ($3d^3$) in both La_2MnNiO_6 and $La_{1.8}Sr_{0.2}MnNiO_6$, and Ni ions are nearly divalent ($3d^8$) in La_2MnNiO_6. A contribution from the Ni^{3+} states has been observed for $La_{1.8}Sr_{0.2}MnNiO_6$, reflecting that the hole carriers, induced by Sr doping, are created mainly at Ni sites. XMCD measurements manifest that the spin moments of Mn and Ni ions are parallel to each other but that the dichroic signals for $x=0.2$ are much smaller than for $x=0$. Our study reveals that hole carriers are created mainly in the Ni $e_g\uparrow$-O 2p-hybridized orbitals to have the metallic behavior in $La_{1.8}Sr_{0.2}MnNiO_6$, which is consistent with the half-metallic ground state obtained from the band calculations for cation-ordered $La_{1.75}Sr_{0.25}MnNiO_6$.

---

*Corresponding author. kangjs@catholic.ac.kr

†Corresponding author. bimin@postech.ac.kr

[1] G. Blasse, J. Phys. Chem. Solids **26**, 1969 (1965).

[2] K. Asai, H. Sekizawa, and S. Iida, J. Phys. Soc. Jpn. **47**, 1054 (1979).

[3] N. S. Rogado, J. Li, A. W. Sleight, and M. A. Subramanian, Adv. Mater. (Weinheim, Ger.) **17**, 2225 (2005).

[4] A. Wold, R. J. Arnott, and J. B. Goodenough, J. Appl. Phys. **29**, 387 (1958).

[5] J. B. Goodenough, A. Word, R. J. Arnott, and N. Menyuk, Phys. Rev. **124**, 373 (1961).

[6] C. L. Bull, D. Gleeson, and K. S. Knight, J. Phys.: Condens. Matter **15**, 4927 (2003).

[7] V. L. Joseph Joly, S. K. Date, and P. A. Joy, J. Phys.: Condens. Matter **16**, 155 (2004).

[8] H. Fujiki and S. Nomura, J. Phys. Soc. Jpn. **23**, 648 (1967).

[9] M. Sonobe and K. Asai, J. Phys. Soc. Jpn. **61**, 4193 (1992).

[10] J. M. Paulsen, C. L. Thomas, and J. R. Dahn, J. Electrochem. Soc. **147**, 861 (2000).

[11] M. C. Sanchez, J. Garcia, J. Blasco, G. Subias, and J. Perez-Cacho, Phys. Rev. B **65**, 144409 (2002).

[12] J. Blasco, M. C. Sanchez, J. Perez-Cacho, J. Garcia, G. Subias, and J. Campo, J. Phys. Chem. Solids **63**, 781 (2002).

[13] M. Sakai, A. Masuno, D. Kan, M. Hashisaka, K. Takata, M. Azuma, M. Takano, and Y. Shimakawa, Appl. Phys. Lett. **90**, 072903 (2007).

[14] V. L. Joseph Joly, P. A. Joy, S. K. Date, and C. S. Gopinath, Phys. Rev. B **65**, 184416 (2002).

[15] R. I. Dass, J.-Q. Yan, and J. B. Goodenough, Phys. Rev. B **68**, 064415 (2003).

[16] F. M. F. de Groot, J. C. Fuggle, B. T. Thole, and G. A. Sawatzky, Phys. Rev. B **42**, 5459 (1990).

[17] G. van der Laan and I. W. Kirkman, J. Phys.: Condens. Matter **4**, 4189 (1992).

[18] S. C. Wi, J.-S. Kang, J. H. Kim, S.-B. Cho, B. J. Kim, S. Yoon, B. J. Suh, S. W. Han, K. H. Kim, K. J. Kim, B. S. Kim, H. J. Song, H. J. Shin, J. H. Shim, and B. I. Min, Appl. Phys. Lett. **84**, 4233 (2004).

[19] B. T. Thole, P. Carra, F. Sette, and G. van der Laan, Phys. Rev. Lett. **68**, 1943 (1992).

[20] C. T. Chen, Y. U. Idzerda, H.-J. Lin, N. V. Smith, G. Meigs, E. Chaban, G. H. Ho, E. Pellegrin, and F. Sette, Phys. Rev. Lett. **75**, 152 (1995).

[21] S. Hüfner, *Photoelectron Spectroscopy, Solid-State Sciences* (Springer-Verlag, Berlin, 1995), Vol. 82.

[22] J.-S. Kang, J. H. Kim, A. Sekiyama, S. Kasai, S. Suga, S. W. Han, K. H. Kim, T. Muro, Y. Saitoh, C. Hwang, C. G. Olson, B. J. Park, B. W. Lee, J. H. Shim, J. H. Park, and B. I. Min, Phys. Rev. B **66**, 113105 (2002).

[23] J.-S. Kang (unpublished).

[24] Mn ions in these reference oxides are all nearly octahedrally coordinated.

[25] C. Mitra, Z. Hu, P. Raychaudhuri, S. Wirth, S. I. Csiszar, H. H. Hsieh, H.-J. Lin, C. T. Chen, and L. H. Tjeng, Phys. Rev. B **67**, 092404 (2003).

[26] P. Ghigna, A. Campana, A. Lascialfari, A. Caneschi, D. Gatteschi, A. Tagliaferri, and F. Borgatti, Phys. Rev. B **64**, 132413 (2001).

[27] $d^{n+2}\underline{L}^2$ configuration is neglected because of the large U_{dd}.

[28] H. Guo, A. Gupta, M. Varela, S. Pennycook, and J. Zhang, Phys. Rev. B **79**, 172402 (2009).

[29] J.-S. Kang, G. Kim, H. J. Lee, S. Kolesnik, B. Dabrowski,

Hangil Lee, J.-Y. Kim, Jieun Lee, Bongjae Kim, and B. I. Min, J. Appl. Phys. **105** 07D721 (2009). $h\nu \approx 639$ eV and $h\nu \approx 643$ eV have been employed in the extraction of Mn $3d$ PES, and $h\nu \approx 854$ eV and $h\nu \approx 856$ eV have been employed in the extraction of Ni $3d$ PES for La_2MnNiO_6.

[30] Ni ions in these oxides are all octahedrally coordinated.

[31] L. A. Montoro, M. Abbate, E. C. Almeida, and J. M. Rosolen, Chem. Phys. Lett. **309**, 14 (1999).

[32] T. Mizokawa, A. Fujimori, T. Arima, Y. Tokura, N. Mori, and J. Akimitsu, Phys. Rev. B **52**, 13865 (1995).

[33] S. F. Matar, M. A. Subramanian, A. Villesuzanne, V. Eyert, and M.-H. Whangbo, J. Magn. Magn. Mater. **308**, 116 (2007).

[34] H. Das, U. V. Waghmare, T. Saha-Dasgupta, and D. D. Sarma, Phys. Rev. Lett. **100**, 186402 (2008).

[35] Bongjae Kim, Jieun Lee, Beom Hyun Kim, Hong Chul Choi, Kyoo Kim, J.-S. Kang, and B. I. Min, J. Appl. Phys. **105** 07E515 (2009).

[36] In the Mn $3d$ and Ni $3d$ PES spectra for both $x=0$ and $x=0.2$, no clear metallic Fermi edges have been observed.

[37] This finding is consistent with resistance measurements, which show at room temperature significantly lower resistance (~ 2 kΩ) for $La_{1.8}Sr_{0.2}MnNiO_6$ compared to ~ 300 kΩ for La_2MnNiO_6 [S. Kolesnik and B. Dabrowski (unpublished)].